Geomechanics and Engineering, *Vol. 24, No. 3 (2021) 295-305*
DOI: https://doi.org/10.12989/gae.2021.24.3.295

Design charts for consolidation settlement of marine clays using finite strain consolidation theory

Sang-Hyun Jun*[1], Jong-Ho Lee[2a], Byung-Soo Park[3b] and Hyuk-Jae Kwon[4c]

[1]*Infra Division, POSCO E&C, 241 Incheon Tower Daero, Incheon, 22009, Korea*
[2]*Department of Civil Engineering, Kyungdong University, Gyeonggi, 11458, Korea*
[3]*Department of Smart City & Civil Engineering, Gangwon State University, Gangwon, 25425, Korea*
[4]*Department of Civil Engineering, Cheongju University, Chungbuk, 28503, Korea*

(Received July 8, 2020, Revised December 24, 2020, Accepted January 27, 2021)

Abstract. In this study, design charts for estimating consolidation settlement are proposed according to finite strain consolidation theory using a nonlinear constitutive relationship equation. Results of parametric sensitivity analysis shows that the final settlement, initial height, and initial void ratio exerted the greatest effect, and the coefficients of the void ratio–effective-stress. Proposed design charts were analyzed for three regions using a representative constitutive relationship equation that enables major dredged-reclaimed construction sites in Korea. The regional design charts can be calculated accurately for the final settlement because it is applied directly to the numerical analysis results, except for reading errors. A general design chart applicable to all marine clays is proposed through correlation analysis of the main parameters. A final self-weight consolidation settlement with various initial void ratios and initial height conditions should be estimated easily using the general design chart and constitutive relationship. The estimated final settlement using the general design chart is similar to the results of numerical analysis obtained using finite strain consolidation theory. Under an overburden pressure condition, design charts for estimating consolidation settlement are proposed for three regions in Korea.

Keywords: design chart; consolidation settlement; finite strain consolidation theory; constitutive relationship equation; parametric sensitivity analysis

1. Introduction

The most critical issue of dredged-reclaimed marine clay is large consolidation settlements. To estimate large settlements, finite strain consolidation theory should be applied instead of small strain consolidation theory. Gibson *et al.* (1967) proposed a finite strain consolidation theory applicable to nonlinear compressibility and permeability. Numerical analysis conducted using the equation that is governed by the finite strain consolidation theory is known to estimate a large consolidation settlement (Stark *et al.* 2005a, Stark *et al.* 2005b, Liu and Griffiths 2015, Hu *et al.* 2018, Liu *et al.* 2019)

Research on finite strain consolidation theory has been performed to solve governing equations by numerical analysis and a solution chart suggested has been for expanding usability. Gibson *et al.* (1981) and Cargill (1984) suggested a solution chart using finite strain consolidation theory. Fox (1999, 2000) proposed a solution chart where linear and nonlinear constitutive relationships are applied for void ratio-effective-stress and void ratio-permeability using the piecewise linear approach method. Morris (2002) studied a solution chart using finite strain consolidation theory with a linear constitutive relationship. Brandenberg (2017) propsed an implicit finite difference code, and deployed through an HTML user interface.

Estimating the consolidation phenomenon by the finite strain consolidation theory is difficult owing to the lack of understanding the theory or the difference in consolidation parameters in Korea. In this study, design charts are proposed to calculate the final consolidation settlement of three regions (Busan, Gwangyang, and Incheon in Korea), which are classified from a major dredged-reclaimed construction site. Furthermore, a general design chart for the final consolidation settlement is proposed for all regions. A design chart of consolidation settlement under overburden pressure is proposed for the three abovementioned regions in Korea.

2. Methodolgy

In this study, constitutive relationship equations for three regions in Korea are applied result of research by Jun & Kwon (2020), as shown in Table 1. The constitutive relationship equation is non-linear relationship between void ratio (e) and effective stress (σ'), void ratio and permeability coefficient (k), and used to estimate the consolidation behavior by the large consolidation

*Corresponding author, Ph.D.
E-mail: clays@poscoenc.com
[a]Professor
E-mail: kwcon@kduniv.ac.kr
[b]Professor
E-mail: claynsand@hanmail.net
[c]Professor
E-mail: hjkwon@cju.ac.kr

ISSN: 2005-307X (Print), 2092-6219 (Online)

Table 1 Representative constitutive relationship equations (Jun and Kwon 2020)

Region		Representative Constitutive Relationship		Applicable Range of Liquid Limits
		Void Ratio-Effective Stress (kPa)	Void Ratio-Permeability (m/day)	
Busan	bs-L-clay	$e = 3.1\ \boldsymbol{\sigma'}^{-0.19}$	$k = 9 \times 10^{-6}\ e^{5.5}$	40~60%
	bs-H-clay	$e = 4.3\ \boldsymbol{\sigma'}^{-0.20}$	$k = 6 \times 10^{-6}\ e^{4.5}$	60~80%
Gwangyang	gy-L-clay	$e = 2.9\ \boldsymbol{\sigma'}^{-0.18}$	$k = 9 \times 10^{-6}\ e^{6.0}$	40~60%
	gy-H-clay	$e = 3.9\ \boldsymbol{\sigma'}^{-0.20}$	$k = 8 \times 10^{-6}\ e^{4.5}$	60~80%
Incheon	ic-L-clay	$e = 1.7\ \boldsymbol{\sigma'}^{-0.15}$	$k = 1 \times 10^{-4}\ e^{5.5}$	20~30%
	ic-H-clay	$e = 2.2\ \boldsymbol{\sigma'}^{-0.17}$	$k = 5 \times 10^{-5}\ e^{5.5}$	30~40%

Table 2 Applied values for parametric sensitivity analysis

Type	Parameters	Symbol	Ranges	Default values
Physical and consolidation properties	Specific gravity of soil solid	G_S	2.60–2.80	2.70
	Unit weight of water (kN/m³)	γ_w	9.81–10.2	10.01
	$e = A\sigma'^{B}$ (σ': kPa)	A	1.0–5.0	3.0
		B	-0.3 to -0.1	-0.2
	$k = Ce^{D}$ (k: m/day)	C	(0.001–1) × 10^{-3}	5 × 10^{-5}
		D	3.0–8.0	5.5
Conditions of reclamation	Initial void ratio	e_0	2.0–30.0	16.0
	Reclaimed initial height (m)	h_0	2.0–30.0	16.0
	Overburden pressure (kPa)	Q	0–200	0

deformation. Jun and Kwon conducted physical experiments for 23 specimens of the main reclaimed-dredged sites in Korea, and proposed 6 representative equations for 3 regions by back-analysis of the centrifugal experiments using finite strain consolidation theory. The bs-L-clay means marine clay of the Busan region having liquid limit of 40-60% range, and the bs-H-clay means marine clay of the Busan region having liquid limit of 60-80%. The gy-L-clay and gy-H-clays mean marine clay of Gwangyang region having liquid limits of 40-60% and 60-80%, respectively. The ic-L-clay and ic-H-clays mean marine clay of Incheon region having liquid limits of 20-30% and 30-40%, respectively.

The six constitutive relationship equations are used to analyze consolidation settlement by self-weight or overburden pressure under the consolidation conditions such as initial void ratio, initial height and so on. The consolidation settlements are estimated by the computer program 'Primary Consolidation, Secondary Compression, and Desiccation of Dredged Fill' (PSDDF) by Stark *et al.* (2005a, 2005b).

3. Sensitivity analysis of the parameters

The parameters for the finite strain consolidation analysis of dredged-reclaimed marine clay are basic physical properties, such as the specific gravity of soil solids and unit weight of water; and consolidation properties, such as void ratio—effective-stress and void ratio-–permeability. In addition, the parameters include those of construction conditions, such as initial void ratio and initial height. Parametric sensitivity analysis was performed to estimate the effects of these parameters on the finite strain consolidation theory.

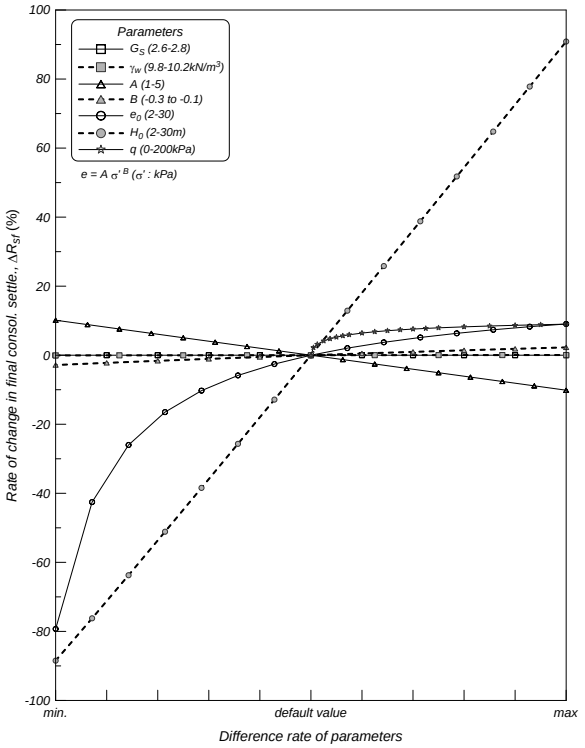

Fig. 1 Parametric sensitivity analysis for final self-weight consolidation settlement

The range and default values of the parameters were applied from the results of laboratory tests and back

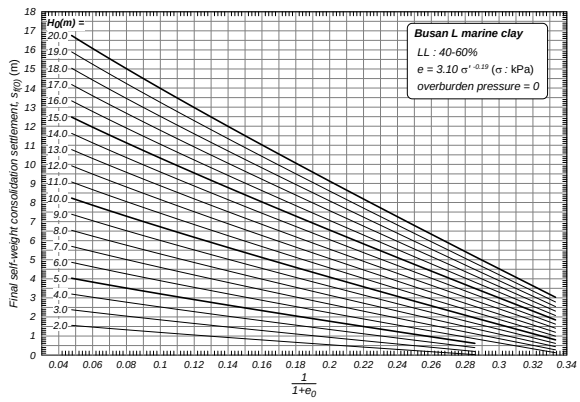

(a) 40%-60% of liquid limit (Busan L clay)

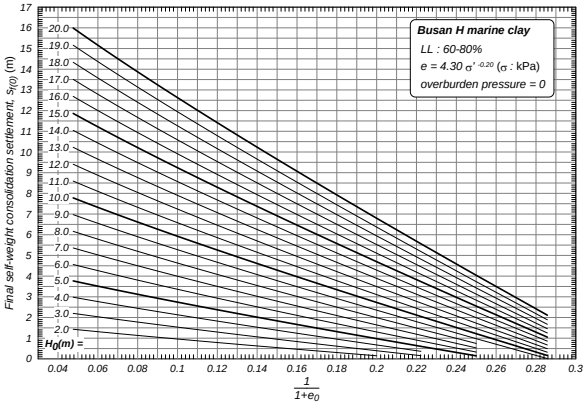

(b) 60%-80% of liquid limit (Busan H clay)

Fig. 2 Final settlement design chart for Busan region

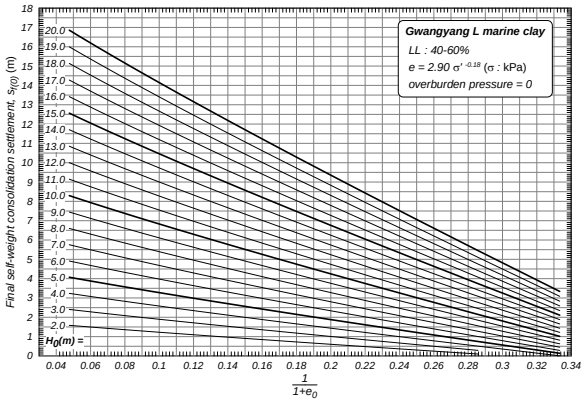

(a) 40%-60% of liquid limit (Gwangyang L clay)

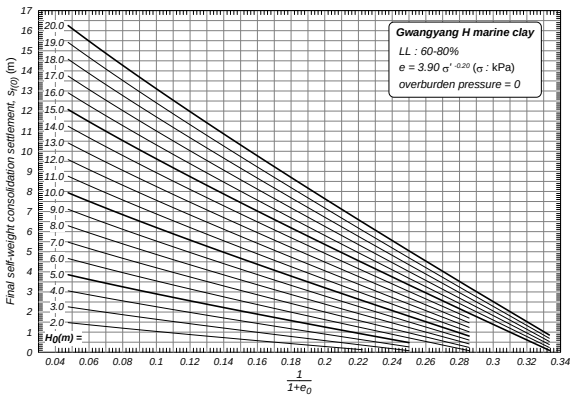

(b) 60%-80% of liquid limit (Gwangyang H clay)

Fig. 3 Final settlement design chart for Gwangyang region

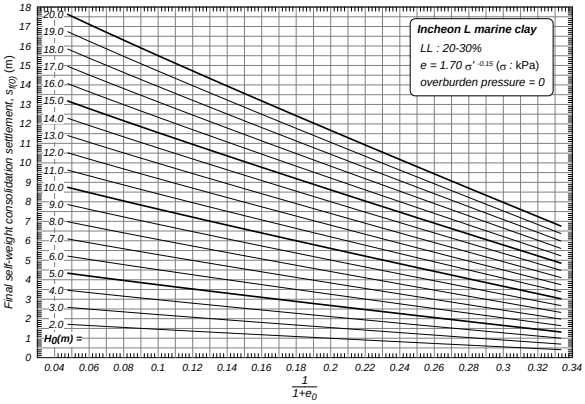

(a) 20%-30% of liquid limit (Incheon L clay)

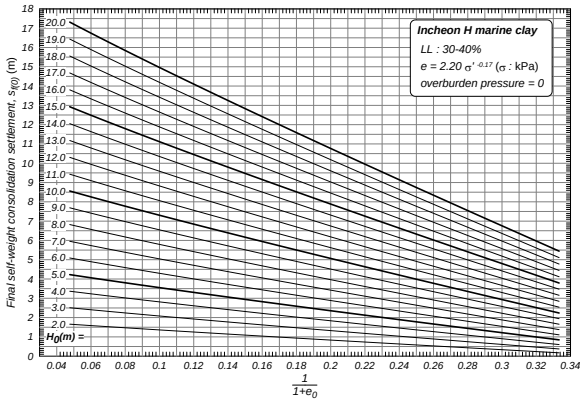

(b) 30%-40% of liquid limit (Incheon H clay)

Fig. 4 Final settlement design chart for Incheon region

analysis using many specimens in-situ by Jun & Kwon (2020), as shown in Table 2. The construction conditions, such as the initial void ratio and initial height, were obtained from actual reclaimed site conditions in Korea.

Fig. 1 shows the results of parametric sensitivity analysis for the final self-weight consolidation settlement. The initial void ratio and initial height exerted the greatest effect. The coefficients for void ratio–effective-stress of constitutive relationships, A and B, imposed a significant effect. The specific gravity of the soil and unit weight of water exerted a relatively small effect, and the coefficients for void ratio-permeability coefficient C and D did not impose any effect. Based on the parametric analysis, coefficients C and D were not considered in the proposal for the design chart of the final settlement, and the specific gravity of the soil solid and unit weight with relatively small effects were applied as representative values.

The relationship between the initial void ratio and final settlement was nonlinear; however, the relationship between $1/(1 + e_0)$ and the final settlement was linear. Therefore, a

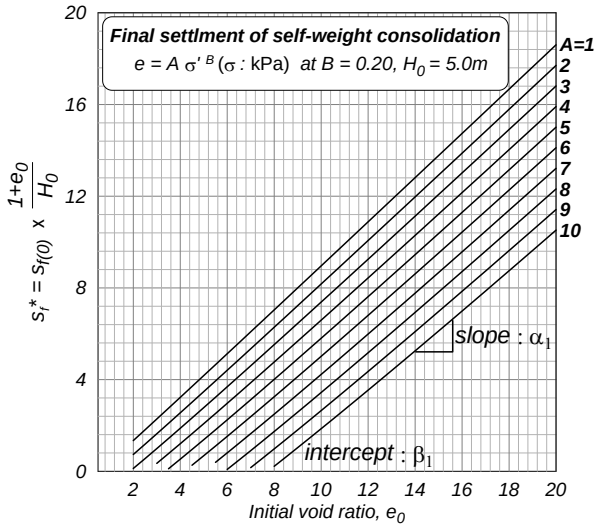

Fig. 5 Normalized final settlement according to initial void ratio

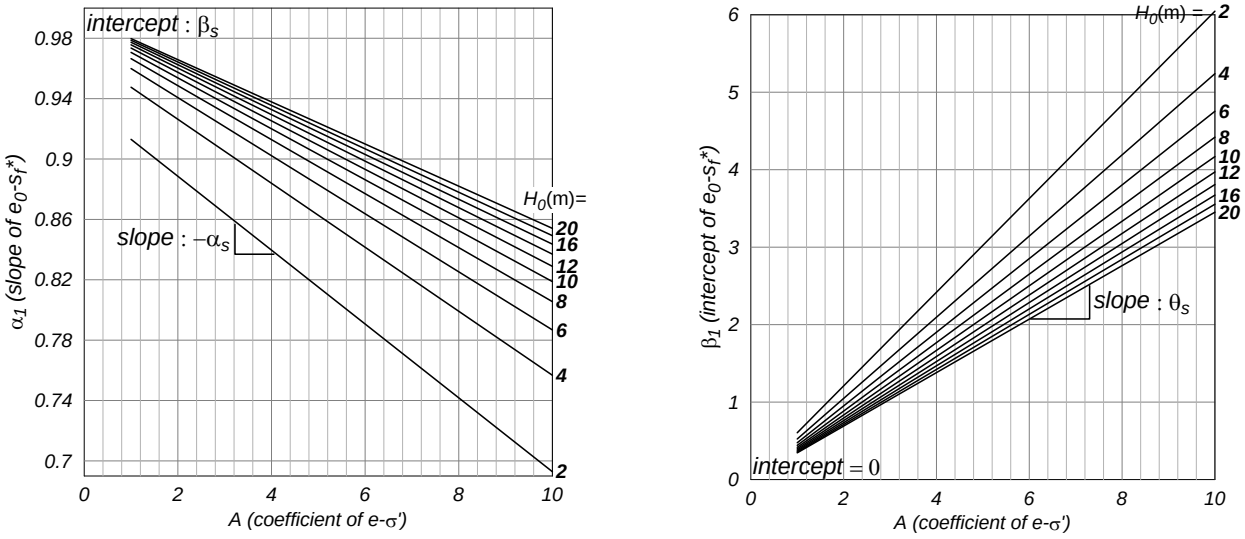

(a) Between A and α_1 (b) Between A and β_1

Fig. 6 Correlation of parameters

design chart of $1/(1 + e_0)$ was suggested instead of that of the initial void ratio.

4. Design charts for the three regions

The design chart for calculating the final consolidation settlement of dredged-reclaimed clay was suggested using the representative constitutive relationship (Jun and Kwon 2020) of the three regions divided into six regions based on liquid limits (LLs) (Busan L clay, Busan H clay, Gwangyang L clay, Gwangyang H clay, Incheon L clay, and Incheon H clay). Fig. 2(a) shows the final self-weight consolidation settlement of the Busan region with 40%-60% of the LL; Fig. 2(b) shows that of the Busan region with 60%–80% of the LL; Fig. 3(a) shows that of the Gwangyang region with 40%-60% of the LL; Fig. 3(b) shows that of the Gwangyang region with 60%-80% of the LL. Figs. 4(a) and 4(b) show the final settlements of Incheon regions with 20%-30% and 30-40% of LL, respectively.

The proposed design chart directly reflects the calculation of finite strain consolidation analysis. Therefore, the final settlement from the design chart can be regarded as the same as the results of numerical analysis.

5. General design chart

5.1 The proposed general design chart

The major parameters affecting the self-weight consolidation settlement $s_{f(0)}$ are coefficients A and B for the void ratio–effective-stress, initial void ratio, and initial height, i.e., $s_{f(0)} = f(A, B, e_0, H_0)$. The relationship between $s_{f(0)}$ and $H_o/(1 + e_0)$ is approximately linear with an intercept of zero. In addition, the relationship between e_0 and $s_f^* = s_{f(0)} \cdot (1 + e_0)/H_0$ for a normalized by void ratio is linear, as shown in Eq. (1) and Fig. 5 at B = 0.2 and H_0 = 5 m.

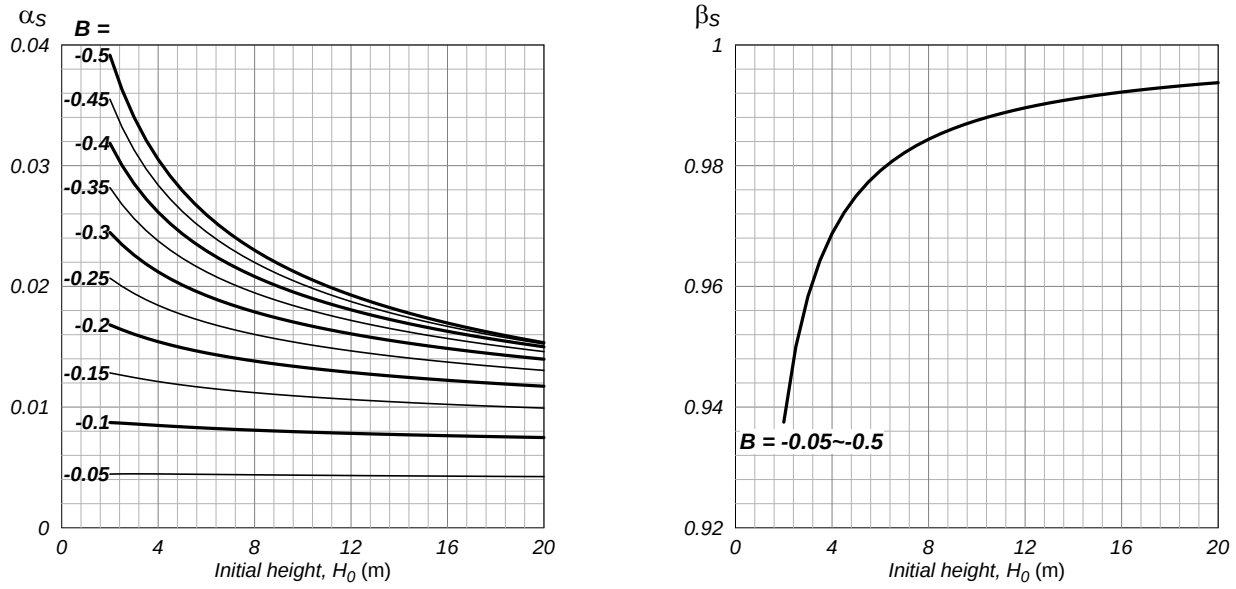

(a) α_s (b) β_s

Fig.7 Analysis of parameters

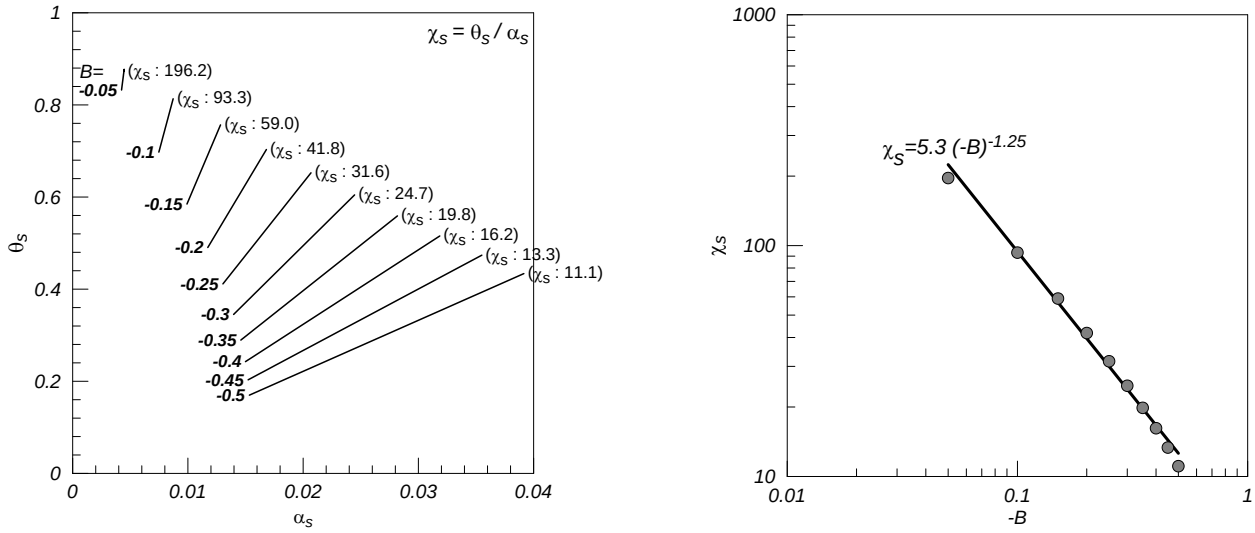

(a) Between α_s and θ_s (b) Between B and χ_s

Fig. 8 Correlation of parameters

$$s_f^* = s_{f(0)} \cdot \frac{1+e_0}{H_0} = \alpha_1 \cdot e_0 - \beta_1 \tag{1}$$

where α_1 is the slope of the linear relationship between e_0 and s_f^*; β_1 is the intercept of the linear relationship between e_0 and s_f^*.

α_1 and β_1 are functions of A, B, and H_0 when it is normalized as e_0. Fig. 6 (a) shows the linear relationship between coefficients A and α_1. The slope and intercept of the linear relationship between A and α_1 are defined as α_s and β_s, respectively. Fig. 6 (b) shows the linear relationship of coefficient A and β_1, with an intercept of zero. The slope of A–β_1 is defined as θ_s. The relationships can be represented by Eqs. (2) and (3). α_s, β_s, and θ_s are functions of B and H_0 because coefficient A is an independent variable.

$$\alpha_1 = -\alpha_s \cdot A + \beta_s \tag{2}$$

$$\beta_1 = \theta_s \cdot A \tag{3}$$

Fig. 7 shows the values of α_s and β_s according to the dependent variables B and H_0. α_s decreases as the initial height increases. The relationship between H_0 and β_s is unique without the variation of coefficient B.

The relationship between α_s and θ_s is linear, with an intercept of zero, as shown in Fig. 8 (a). The slope of α_s and θ_s is defined as χ_s, as shown in Eq. (4); χ_s is a function of coefficient B. The relationship between $\chi_s$and B indicates a power function, as shown in Fig. 8 (b), and the determination coefficient R^2 of the relationship is estimated to be 0.995.

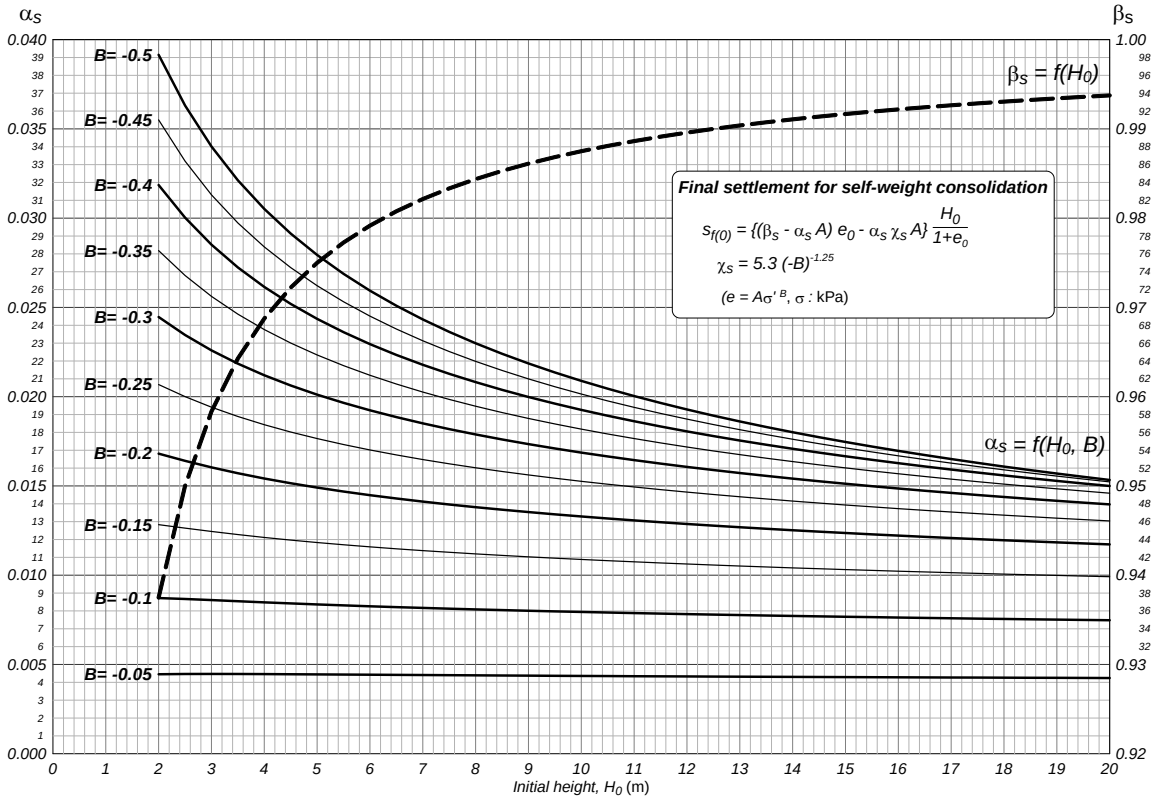

Fig. 9 General design chart of final self-weight consolidation settlement

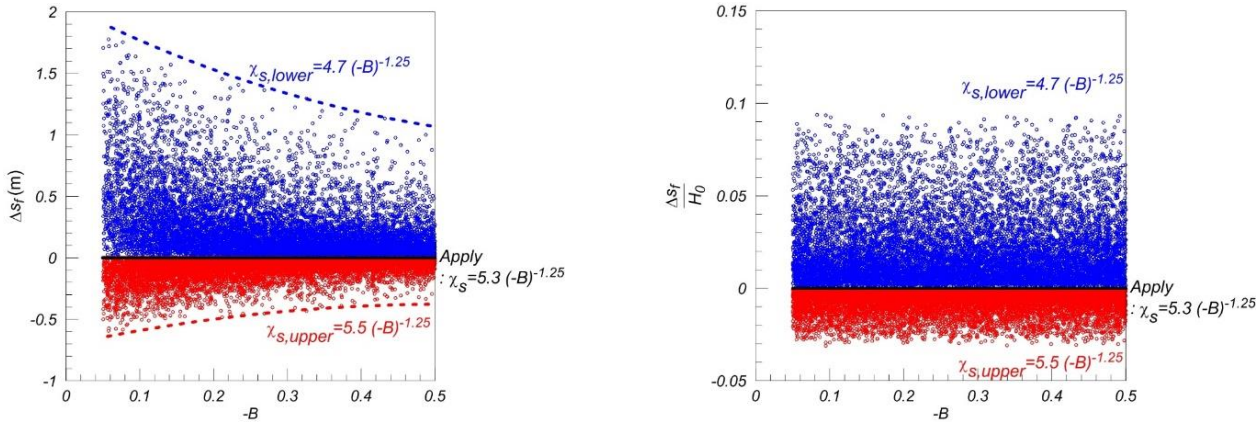

(a) Between B and Δs_f (b) Between B and $\frac{\Delta s_f}{H_0}$

Fig. 10 Error ranges of the proposed general design chart

$$\chi_s = \frac{\theta_s}{\alpha_s} \simeq 5.3 \cdot (-B)^{-1.25} \qquad (R^2 = 0.995) \tag{4}$$

Eq. (5) is derived by substituting Eqs. (2), (3) and (4) into Eq. (1).

$$s_{f(0)} \frac{1+e_0}{H_0} = (\beta_s - \alpha_s A)e_0 - \alpha_s \chi_s A$$
$$s_{f(0)} = [(\beta_s - \alpha_s A)e_0 - \alpha_s \chi_s A] \frac{H_0}{1+e_0} \tag{5}$$

In Eq. (5), α_s and β_s are functions of B, which are the coefficient of void ratio and effective stress, and the initial height, respectively. χ_s is a function of B. Therefore, a general design chart for final self-weight consolidation settlement is proposed as shown in Fig. 9. α_s and β_s can be obtained from B and H_0, and χ_s can be calculated from the power function of Eq. (4) in the design chart.

The design chart of Fig. 9 can be applied in the preliminary design stage using a nearby constitutive relationship equation of void ratio–effective-stress or in the construction stage for calculating the final settlement in situ. The design chart included errors because some relationships were assumed to be linear, and the relationship between B and χ_s was assumed to be a power function. The estimated error range was 10% lower than that of the numerical solution, as shown in Fig. 10.

Table 3 Clay properties and experimental conditions for Yamagami *et al.* (2000)

Soil properties		Sample mud A of Naruto coast		
Physical properties		Gs : 2.704, PI : 40.1%		
Constitutive relationship equations Void ratio - effective stress (kPa)		$e = 2.631\sigma'^{-0.226}$		
Centrifuge and Analysis conditions	Test	AC1	AC2	AC3
	Initial void ratio	6.65	6.65	19.94
	Initial height (m)	9.0	18.0	9.72
Final settlement by numerical analysis of finite strain consolidation theory (m)		5.77	12.11	8.20

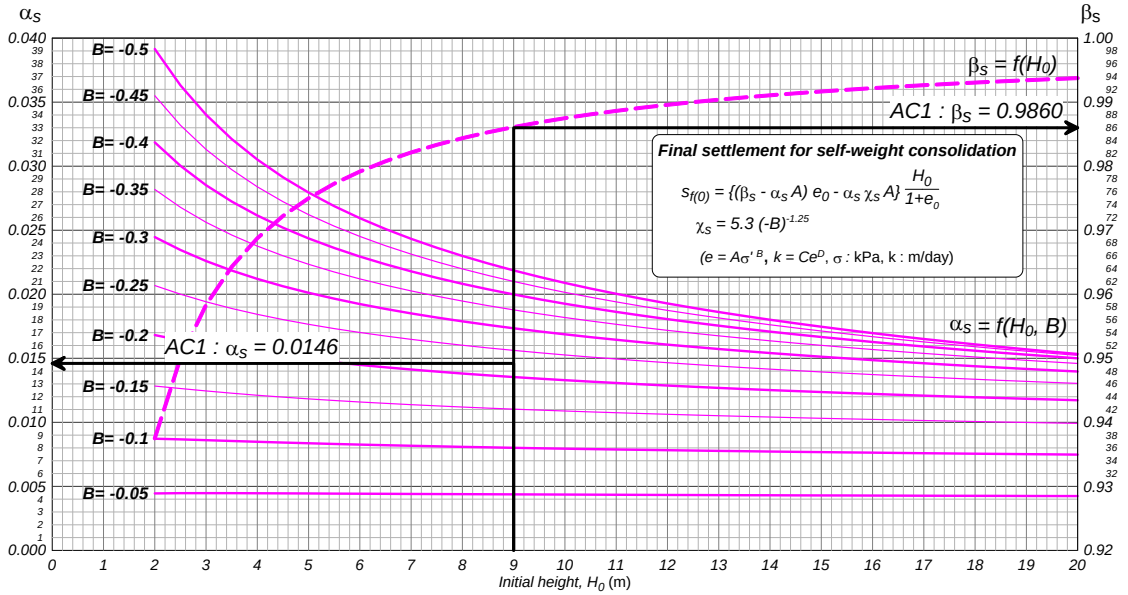

Fig. 11 Estimation of final settlement by general design chart (AC1 case)

Table 4 Clay properties and analysis conditions for Kim (2006)

Soil properties		Sample mud A of Naruto coast	
Physical properties	Gs	2.70	2.69
	LL (%)	47.21±2	55.85±2
	PI (%)	20.68±2	32.30±2
	Void ratio - effective stress (kPa)	$e = 6.72\sigma'^{-0.31}$	$e = 6.04\sigma'^{-0.27}$
Constitutive relationship equations Void ratio - effective stress (kPa)		$e = 2.631\sigma'^{-0.226}$	
Analysis conditions	Initial void ratio	8.10	8.07
	Initial height (m)	8.60	7.93
Final settlement by numerical analysis of finite strain consolidation theory (m)		3.86	3.55

5.2 Application of the general design chart

Yamagami *et al.* (2000) calculated consolidation settlements using specimens from the coast of Naruto in the East of the Tokushima prefecture. The properties and final self-weight consolidation settlement of clay are shown in Table 3.

The final settlements of three cases (AC1, AC2, and AC3 in Table 3) were calculated using the general design chart. α_s and β_s can be read from the general design chart shown in Fig. 11. The values of α_s were 0.0146, 0.0127, and 0.0144 in AC1, AC2, and AC3, respectively. The read values of β_s were 0.9860, 0.9930, and 0.9872 in AC1, AC2, and AC3, respectively. χ_s was 34.01, which is the calculated suggested power function (χ_s = 5.3(-B) -1.25 = 5.3(0.226) -1.25 = 34.01). The final settlements were 5.88, 12.34, and 8.19 m in AC1, AC2, and AC3, respectively, which were calculated using Eq. (5) using the read parameters. These values were similar to 5.77 and 5.88 m in AC1; 12.11 and 12.34 m in AC2; and 8.19 and 8.20 m in AC3.

Kim (2006) analyzed consolidation behavior of the Gwangyang marine clay in Korea. The properties and final

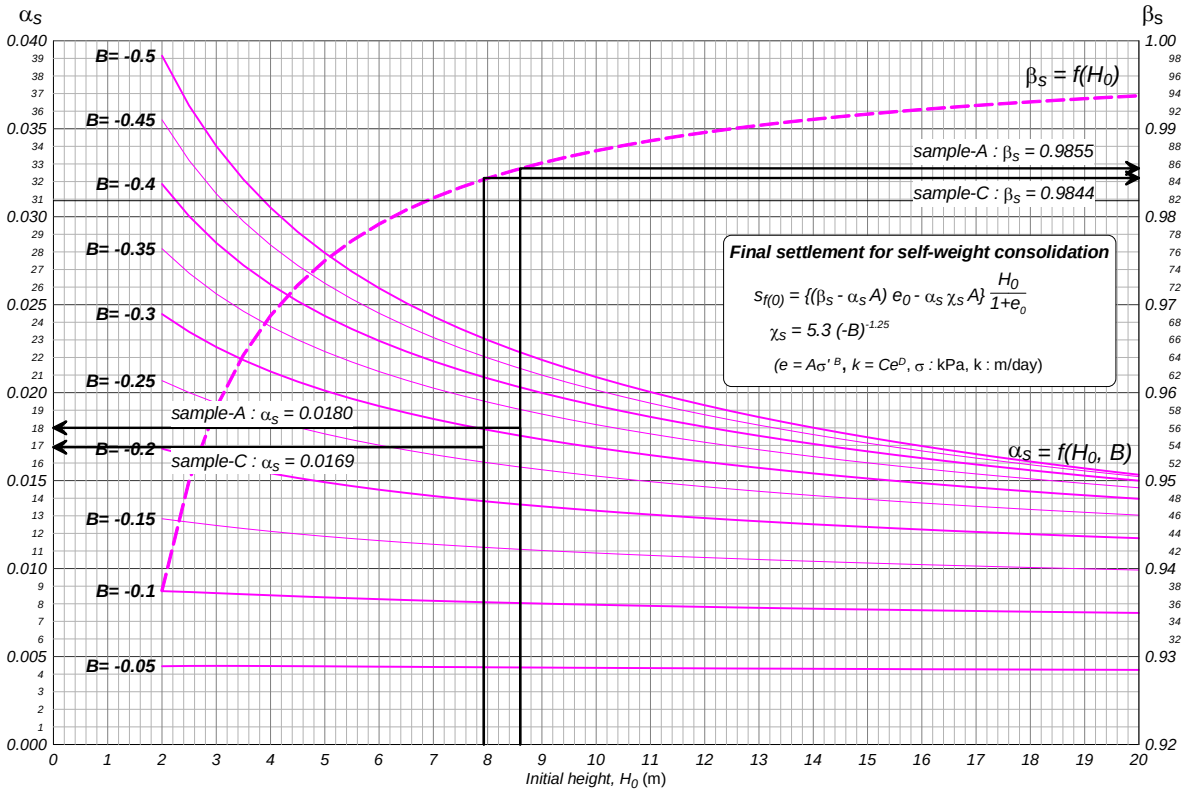

Fig. 12 Estimation of final settlement by general design chart (Sample-A and Sample-C)

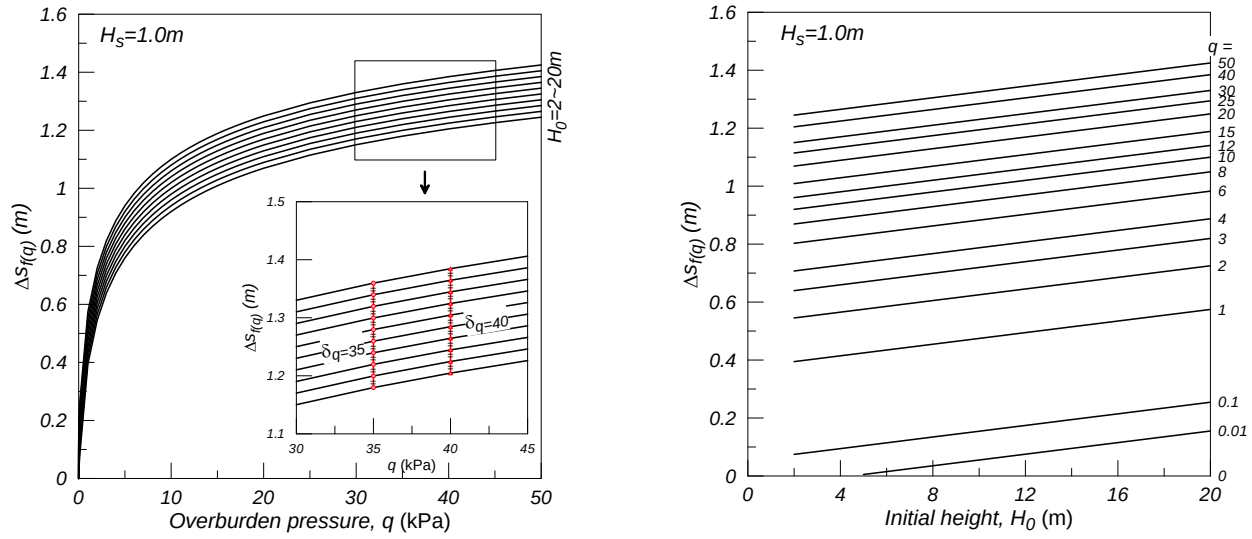

(a) Addition settlement by overburden pressure (b) Additional settlement as the initial height

Fig. 13 Correlation for overburden pressure at H_s = 1 for Busan L clay

self-weight consolidation settlement of clay are shown in Table 4.

The final settlements of two cases (Sample-A, Sample-C in Table 4) were calculated using the general design chart. α_s and β_s can be read from the general design chart shown in Fig. 12. The values of α_s were 0.0180 and 0.0169 in Sample-A and Sample-C, respectively. The read values of β_s were 0.9855 and 0.9844 in Sample-A and Sample-C, respectively. χ_s values were 22.96 and 27.26 in Sample-A and Sample-C, respectively, which are calculated by Eq. (4). The final settlements were 3.99 and 3.79 m in Sample-A and Sample-C, respectively, which were calculated using Eq. (5) using the read parameters. These values were similar to 3.86 and 3.99 m in Sample-A; and 3.55 and 3.79 m in Sample-C.

6. Design chart for overburden pressure

An overburden pressure induces an additional consolidation settlement ($\Delta s_{f(q)}$) of clay. The additional consolidation settlement by an overburden pressure was

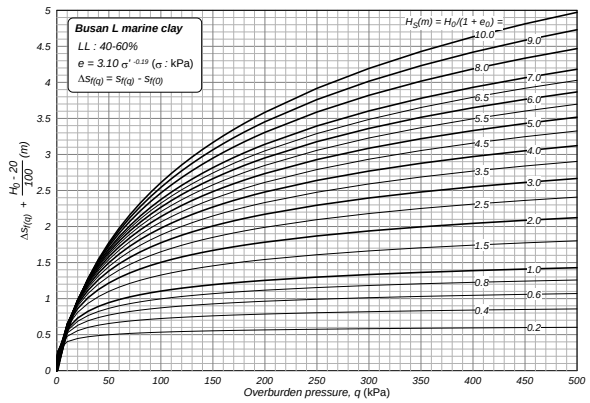

(a) 40%-60% of liquid limit (Busan L clay)

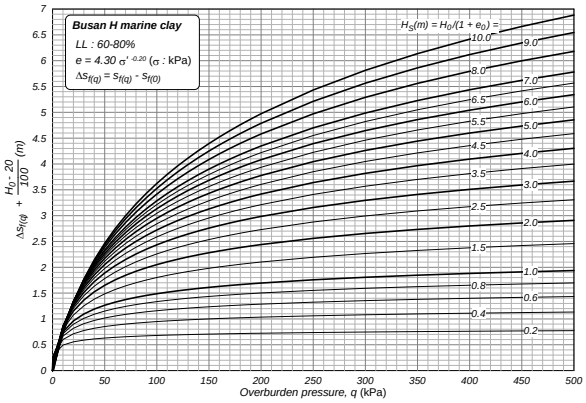

(b) 60%-80% of liquid limit (Busan H clay)

Fig. 14 Design chart of final settlement by overburden pressure (Busan region)

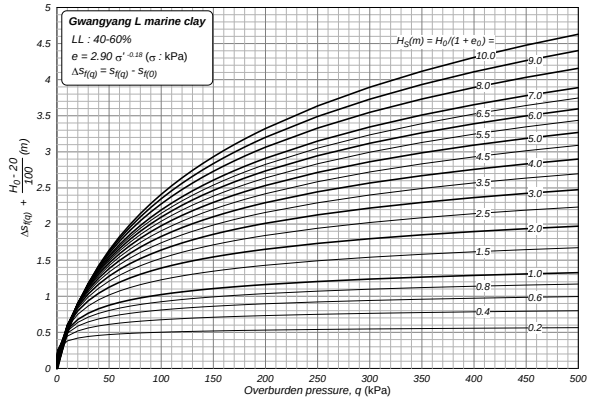

(a) 40%-60% of liquid limit (Gwangyang L clay)

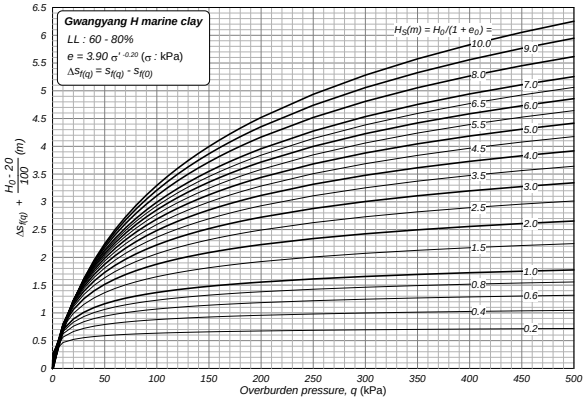

(b) 60%-80% of liquid limit (Gwangyang H clay)

Fig. 15 Design chart of final settlement by overburden pressure (Gwangyang region)

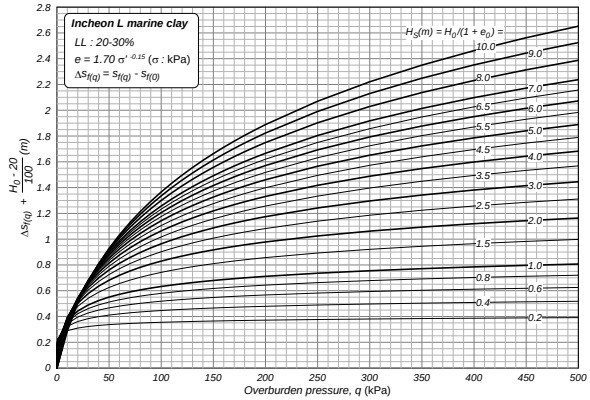

(a) 20%-30% of liquid limit (Incheon L clay)

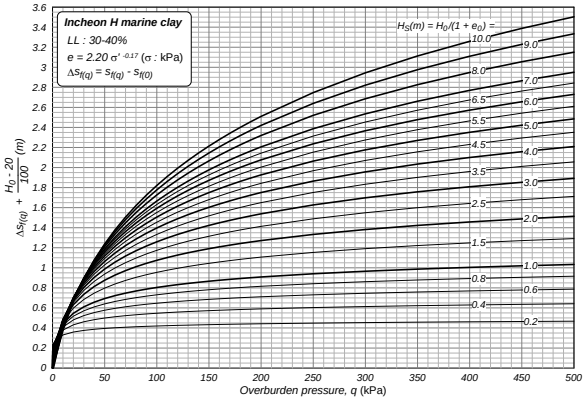

(b) 30%-40% of liquid limit (Incheon H clay)

Fig. 16 Design chart of final settlement by overburden pressure (Incheon region)

analyzed for various heights of the solid. The height of the solids (H_s) is defined as $H_0/(1+\mathrm{e}_0)$. The analysis results for the case of H_s = 1 for Busan L marine clay is shown in Fig. 13. $\Delta s_{f(q)}$ increased nonlinearly with the overburden pressure (q). The variable amounts of $\Delta s_{f(q)}$ by the variable initial height were the same, as shown in the small box in Fig. 13(a). $\Delta s_{f(q)}$ was governed linearly according to the variation in the initial height, as shown in Fig. 13(b). The tendency was similar regardless of the change in the height of the solids, i.e., when an additional settlement by overburden pressure is provided by the height of solids at a standard initial height, the additional settlement can be calculated in any condition.

Design charts based on the overburden pressure are proposed, as shown in Figs. 14-16. The standard initial height was set to 20 m for the proposition as a positive number. To estimate the additional settlement by the overburden pressure, the self-weight consolidation settlement should be calculated first. The height of the solids was calculated by the initial height and initial void

ratio. Subsequently, the Y-axis value was read from Figs. 14-16. The final settlement by the self-weight and overburden can be calculated using the following equation:

$$s_{f(0)} = s_{f(0)} + Y_{axis\_value} - \frac{(H_0 - 20)}{100} \quad (6)$$

7. Conclusions

In the present study, design charts were proposed for easily estimating consolidation settlements according to finite strain consolidation theory using a nonlinear constitutive relationship equation. For the proposed design chart, the effects of parameters on the final settlement were analyzed. Parametric sensitivity analysis indicated that the order of the initial height, initial void ratio, and coefficients of the constitutive relationship equations A and B exerted a significant effect on the final settlement. These results can be applied to select the major parameters for the design chart. From the constitutive relationship equation of void ratio–effective-stress on dredged-reclaimed marine clay construction sites, regional design charts were proposed to estimate the final settlement under various initial conditions. The regional design chart comprised numerical analysis results and can be used to accurately calculate the final settlement. A general design chart was proposed by the correlation between parameters and was applied to all marine clays. The final self-weight consolidation settlement with various initial void ratios and initial height conditions can be estimated easily using the general design chart and constitutive relationship. The estimated final settlement by the general design chart was confirmed to be similar to the results of numerical analysis obtained using finite strain consolidation theory. Under an overburden pressure condition, design charts for estimating consolidation settlement were proposed for three regions in Korea. For the future study, a design chart for the consolidation degree according to the time will be proposed. These design charts will be able to estimate the settlement according to the consolidation time.

References

Au, F.T.K. and Du, J.S. (2004), "Prediction of ultimate stress in un-bonded prestressed tendons", *Mag. Concrete Res.*, **56**(1), 1-11. https://doi.org/10.1680/macr.2004.56.1.1

Azad, A.K., Ahmad, S. and Al-Gohi, B.H.A. (2010), "Flexural strength of corroded reinforced concrete beams", *Mag. Concrete Res.*, **62**(6), 405-414. https://doi.org/10.1680/macr.2010.62.6.405.

Azad, A.K., Ahmad, S. and Azher, S.A. (2007), "Residual strength of corrosion-damaged reinforced concrete beams", *ACI Mater. J.*, **104**(1), 40-47.

Broomfield, J. (1997), *Corrosion of Steel in Concrete: Understanding, Investigating and Repair*, E & FN Spon, London, U.K.

Cairns, J. and Zhao, Z. (1993), "Behaviour of concrete beams with exposed reinforcement", *Proc. Inst. Civ. Eng. Struct. Build.*, **99**(2), 141-154. https://doi.org/10.1680/istbu.1993.23373.

CEB-FIP, CEB-FIP Model Code 1990 (1990), *Design Code*, Thomas Telford, London, U.K.

Chen, H.P. and Xiao, N. (2012), "Analytical solutions for corrosion-induced cohesive concrete cracking", *J. Appl. Math.* https://doi.org/10.1155/2012/769132.

Chen, H.P. (2016), "Monitoring based reliability analysis of aging concrete structures by Bayesian updating", *J. Aerosp. Eng.*, **30**(2), B4015004. https://doi.org/10.1061/(ASCE)AS.1943-5525.0000587.

Chen, H.P. and Alani, A.M. (2012), "Reliability and optimised maintenance for sea defences", *Proc. Inst. Civ. E. Marit. Eng.*, **165**(2), 51-64. https://doi.org/10.1680/maen.2010.37.

Chen, H.P. and Alani, A.M. (2013), "Optimized maintenance strategy for concrete structures affected by cracking due to reinforcement corrosion", *ACI Struct. J.*, **110**(2), 229-238.

Chen, H.P. and Nepal, J. (2015), "Stochastic modelling and lifecycle performance assessment of bond strength of corroded reinforcement in concrete", *Struct. Eng. Mech.*, **54**(2), 319-336. https://doi.org/10.12989/sem.2015.54.2.319.

Chen, H.P. and Nepal, J. (2016), "Analytical model for residual bond strength of corroded reinforcement in concrete structures", *J. Eng. Mech.*, **142**(2), 04015079-1-8. https://doi.org/10.1061/(ASCE)EM.1943-7889.0000997.

Chung, L., Najm, H. and Balaguru, P. (2008), "Flexural behavior of concrete slabs with corroded bars", *Cement Concrete Compos.*, **30**(3), 184-193. https://doi.org/10.1016/j.cemconcomp.2007.08.005.

Coronelli, D. (2002), "Corrosion cracking and bond strength modelling for corroded bars in reinforced concrete", *ACI Struct. J.*, **99**(3), 267-276.

Coronelli, D. and Gambarova, P.G. (2000), "A mechanical model for bond strength of corroded reinforcement in concrete", *Proceedings of the 14th Engineering Mechanics Conference*, Austin, Texas, U.S.A., May.

Du, Y.G., Clark, L.A. and Chan, A.H.C. (2005), "Residual capacity of corroded reinforcing bars", *Mag. Concrete Res.*, **57**(3), 135-147. https://doi.org/10.1680/macr.2005.57.3.135.

Eurocode 2 (2004), Design of Concrete Structure, European Committee for Standardization, Brussels, Belgium.

Fang, C., Lundgren, K., Chen. L. and Zhu, C. (2004), "Corrosion influence on bond in reinforced concrete", *Cement Concrete Res.*, **34**(11), 2159-2167. https://doi.org/10.1016/j.cemconres.2004.04.006.

Giuriani, E., Plizzari, G. and Schumm, C. (1991), "Role of stirrups and residual tensile strength of cracked concrete on bond", *J. Struct. Eng.*, **117**(1), 1-18. https://doi.org/10.1061/(ASCE)0733-9445(1991)117:1(1).

Horringmoe, G., Saether, I., Antonsen, R. and Arntsen, B. (2007), "Laboratory investigations of steel bar corrosion in concrete: Sustainable Bridges Background document SB3.10", Sustainable Bridge, Nourt Technology.

Khan, I., Francois, R. and Castel, A. (2014), "Prediction of reinforcement corrosion using corrosion induced cracks width in corroded reinforced concrete beams", *Cement Concrete Res.*, **56**, 84-96. https://doi.org/10.1016/j.cemconres.2013.11.006.

Law, D.W., Tang, D., Molyneaux, T.K.C. and Gravina, R. (2011), "Impact of crack width on bond: Confined and unconfined rebar", *Mater. Struct.*, **44**(7), 1287-1296. https://doi.org/10.1617/s11527-010-9700-y.

Mangat, P.S. and Elgarf, M.S. (1999), "Flexural strength of concrete beams with corroding reinforcement", *ACI Struct. J.*, **96**(1), 149-159.

Nepal, J. and Chen, H.P. (2015), "Risk-based optimum repair planning of corroded reinforced concrete structures", *Struct. Monitor. Mainten.*, **2**(2), 133-143. http://doi.org/10.12989/smm.2015.2.2.133.

Shang, H.S., Yi, T.H. and Yang, L.S. (2012), "Experimental study on the compressive strength of big mobility concrete with non-destructive testing method", *Adv. Mater. Sci. Eng.*

https://doi.org/10.1155/2012/345214.
Tilly, G.P. and Jacobs, J. (2007), *Concrete Repairs-Performance in Service and Current Practice*, Willoughby Road, IHS BRE Press, U.K.
Van Noortwijk, J.M. (2009), "A survey of the application of gamma processes in maintenance", *Reliab. Eng. Syst. Safety*, **94**(1), 2-21. https://doi.org/10.1016/j.ress.2007.03.019.
Vidal, T., Castel, A. and Francois, R. (2004), "Analyzing crack width to predict corrosion in reinforced concrete", *Cement Concrete Res*., **34**(1), 165-174. https://doi.org/10.1016/S0008-8846(03)00246-1.
Wang, X.H. and Liu, X.L. (2010), "Simplified methodology for the evaluation of residual strength of corroded reinforced concrete beams", *J. Perform. Constr. Facilit*., **24**(2), 108-119. https://doi.org/10.1061/(ASCE)CF.1943-5509.0000083.
Wang, X.H. and Liu, X.L. (2004), "Modelling effects of corrosion on cover cracking and bond in reinforced concrete", *Mag. Concrete Res*., **56**(4),191-199. https://doi.org/10.1680/macr.2004.56.4.191.
Yalciner, H., Eren, O. and Sensoy, S. (2012), "An experimental study on the bond strength between reinforcement bars and concrete as a function of concrete cover strength and corrosion level", *Cement Concrete Res*., **42**(5), 643-655. https://doi.org/10.1016/j.cemconres.2012.01.003.
Yi, T.H., Li, H.N. and Wang, C.W. (2016), "Multiaxial sensor placement optimization in structural health monitoring using distributed wolf algorithm", *Struct. Contr. Health Monitor*., **23**(4), 719-734. https://doi.org/10.1002/stc.1806.
Zhang, R., Castel, A. and François, R. (2010), "Concrete cover cracking with reinforcement corrosion of RC beam during chloride-induced corrosion process", *Cement Concrete Res*., **40**(3), 415-425. https://doi.org/10.1016/j.cemconres.2009.09.026.
Zhao, Y., Lin, H., Wu, K. and Jin, W. (2013), "Bond behaviour of normal/recycled concrete and corroded steel bars", *Constr. Build. Mater*., **48**, 348-359. https://doi.org/10.1016/j.conbuildmat.2013.06.091.

JS